



DC Electric Fields Induce Perpendicular Alignment and Enhanced Migration in Schwann Cell Cultures

SPENCER J. BUNN,^{1,2} ALEXANDER LAI,^{1,2} and JIANMING LI^{1,3}

¹Center for Paralysis Research, Purdue University, West Lafayette, IN 47907, USA; ²Department of Biomedical Engineering, Purdue University, West Lafayette, IN 47907, USA; and ³Department of Basic Medical Sciences, Purdue University, West Lafayette, IN 47907, USA

(Received 14 November 2018; accepted 29 March 2019; published online 8 April 2019)

Associate Editor Joel Stitzel oversaw the review of this article.

Abstract—Schwann cells (SCs) are PNS glia that play numerous support functions including myelination of axons. After PNS injury, SCs facilitate regeneration by phagocytosing cellular debris and providing physical and biochemical cues to guide axon growth. This reparative phenotype suggests SCs could be critical cellular targets for enhancing nerve regeneration. One method for altering cell morphology and motility is the application of direct current (DC) electric fields (EFs). Endogenous EFs have physiologic relevance during embryogenesis and serve as guidance and polarization cues. While much literature exists on EFs and CNS and PNS neurons, the effects of EFs on SCs have not been extensively studied. In this work, cell alignment, migration, and morphology of rat SCs were measured in response to several EF stimulation regimes including constant DC, 50% duty cycle DC and oscillating DC. SCs were found to re-orient perpendicular to field lines and respond to DC EFs as low as 75 mV/mm. EF exposure promoted directed migration, with travel towards the cathode at a mean rate of 7.5 $\mu\text{m}/\text{h}$. The data highlight the utility of EFs in modulating SC morphology, alignment and migration. Results may have implications for using EFs to attract and realign SCs at the site of PNS trauma.

Keywords—Galvanotaxis, Electrotaxis, Peripheral nerve repair, Voltage gradient, Bands of Bungner.

INTRODUCTION

Each year, an estimated 42,000–74,000 peripheral nerve injuries (PNIs) occur in the United States,²¹ resulting in localized loss of sensation, motor function and neuropathic pain that significantly impact quality of life. In PNI pathophysiology, nerve segments distal to the injury site undergo Wallerian degeneration

where damaged axons and residual myelin are decomposed. Treatments for PNI depend on the type and severity of the injury. In nerve severance, the most common treatment re-apposes the proximal and distal ends of the nerve (neurorrhaphy). If PNI results in a large distance between the proximal and distal nerve fibers, a nerve graft is used to bridge the gap to minimize tension on the nerve fibers. The current gold standard for nerve repair is the autologous graft. However, functional recovery remains low especially for large gap injuries. Typically, only 20–40% of victims achieve good sensory and motor function following PNI.²² Further, nerve autografts risk donor site morbidity. Allografts, decellularized xenografts and synthetic grafts have also been used, though they are markedly inferior to autologous grafts.³⁷ Recovery of PNI has advanced little in the previous decades, and there exists a need for improvement.

Schwann cells (SCs) have emerged as a potential therapeutic target to enhance axonal regeneration. Following PNI, denervated SCs de-differentiate to a repair phenotype; the SCs become elongated and protein expression changes to support axon regeneration.¹⁸ SCs provide guidance cues by depositing extracellular matrix, forming Bands of Bungner and secreting neurotrophic factors.^{10,11} A significant reduction in axon regrowth was noted when SC population was depleted in mice.¹⁵ Other results suggest that SCs may be a rate limiting step in axon regeneration, especially across the lesion.^{14,38}

Subsequently, we hypothesize that DC electric fields (EFs) may be used as a tool to manipulate SC orientation and possibly, recruit more SCs to the injury site. DC EFs have been shown to influence cell differentiation,¹² alignment,¹⁹ migration,³⁹ gene expression⁴¹ and growth.³⁰ *In vivo*, endogenous EFs play a role in

Address correspondence to Jianming Li, Center for Paralysis Research, Purdue University, West Lafayette, IN 47907, USA. Electronic mail: li128@purdue.edu

embryonic development in many species with typical EF magnitudes ranging from a few mV/mm to 500 mV/mm.^{17,36} The mechanism(s) in which cells respond to EFs are not well understood. Prevailing theories suggest an electrophoretic phenomenon whereby the imposed fields induce asymmetric redistribution of various charged membrane molecules such as cell adhesion proteins, receptor proteins, and ion channels.³ Additionally, EFs may initiate a host of downstream signaling events that alter the cytoskeleton dynamics.⁴²

Several studies have investigated the effects of continuous DC EFs on Schwann cells.^{19,20,41} However, constant DC stimulation is problematic to apply *in vivo* due to electrochemical byproducts generated at the electrode interfaces.⁴ In this work, we propose using alternative stimulation waveforms. Specifically, we assessed: (i) constant DC, (ii) 50% duty cycle DC where the EF was on for 15 min then off for 15 min, and (iii) oscillating DC where the EF was applied constantly but the polarity was reversed every 15 min. Magnitudes of the EFs ranged from 10 to 500 mV/mm. These waveforms have been previously shown to promote axonal extension and regeneration *in vitro* as well as in animals subjected to CNS injury.^{7,8} However, the outcomes of discontinuous waveforms on glia are unknown. Using rat RT4 Schwann cells as a model, we monitored cellular morphology, orientation and migration with time-lapse microscopy and digital image tracking. Cytoskeletal arrangement and cell adhesion proteins were observed with fluorescent microscopy. The experimental results provide guiding parameters that may aid in developing implantable stimulators for enhancing nerve regeneration post-PNI.

EXPERIMENTAL METHODS

SC culture and EF Setup

Immortal RT4 rat SCs (ATCC) were used in this study. Primary SCs used for validation of the RT4 SC line were obtained from Sprague Dawley rats used in a separate study in accordance with regulations set forth by the Purdue Animal Care and Use Committee. In preparation for EF experiments, cells were detached from culture flasks using 0.25% Trypsin EDTA, centrifuged, and resuspended in penstrep media [basal media + 1% penicillin/streptomycin (Sigma-Aldrich)] to a concentration of 1×10^5 cells/mL. Cell suspension containing 10,000 cells (100 μ L) was pipetted into the channel of an IBIDI μ -channel Slide 1. Penstrep media (1 mL) was added to each well of the channel slide. Each well was covered with plastic caps, then the slide was incubated at 37 °C and 5% CO₂ overnight.

After a 16-h incubation period, slides were placed under an Olympus IX81 microscope with a Weatherstation temperature control system (Precision Control) to maintain constant temperature and CO₂ levels. DC EFs were applied through the media using a custom constant current generator. One end of a salt bridge (2% agar/penstrep media in 0.4 cm ID glass tubes, 15 cm length) was placed in each well of the slide. Two glass vials containing the opposing end of the salt bridges and penstrep media (13 mL) were placed next to each well. An electroplated silver/silver chloride electrode was inserted into each vial, and the electrodes were connected to the positive and negative terminals of the current generator. The EF setup (Fig. 1a) allowed for application of EFs of varying strengths without producing cytotoxic byproducts in the channel or wells of the slide. EF strengths of 10, 75, 200 and 500 mV/mm were tested, and SCs without EF exposure (0 mV/mm) were used as controls. The dimensions of the channel slide were constant, so the EF strength was controlled by adjusting the current supplied to the system. Currents used were 0.03 mA (10 mV/mm), 0.24 mA (75 mV/mm), 0.64 mA (200 mV/mm) and 1.60 mA (500 mV/mm).

Three waveforms were used in this study: constant DC EF (Con EF), 50% duty cycle DC EF (50% d.c. EF), and oscillating DC EF (Osc EF) (Fig. 1b). The 50% d.c. EF waveform was achieved by switching the current generator on for 15 min then off for 15 min. In the Osc EF waveform, the field polarity was reversed every 15 min. For all waveforms, the duration of the experiment was 6 h. The current was monitored throughout the experiment (2 Hz sampling frequency). Following EF exposure, the media was aspirated, and cells were fixed with 4% paraformaldehyde solution (1 mL) for 20 min.

Migration

Time-Lapse Image Collection

Phase contrast images were taken during EF exposure using an Olympus IX81 microscope. MetaMorph Premier Version 7.7.4.0 (Molecular Devices) was used to automate image collection at five random positions on each slide every minute. Once images had been collected, time-lapse videos were rendered using Adobe Premier Pro 2017.

Migration Tracking

To track cell migration, every 10th image was loaded into FIJI Version 1.52b, and the Manual Tracking plugin was used (Fig. 1c). The center of each nucleus was manually selected at each timepoint, and the coordinates were used to calculate distance, X-dis-

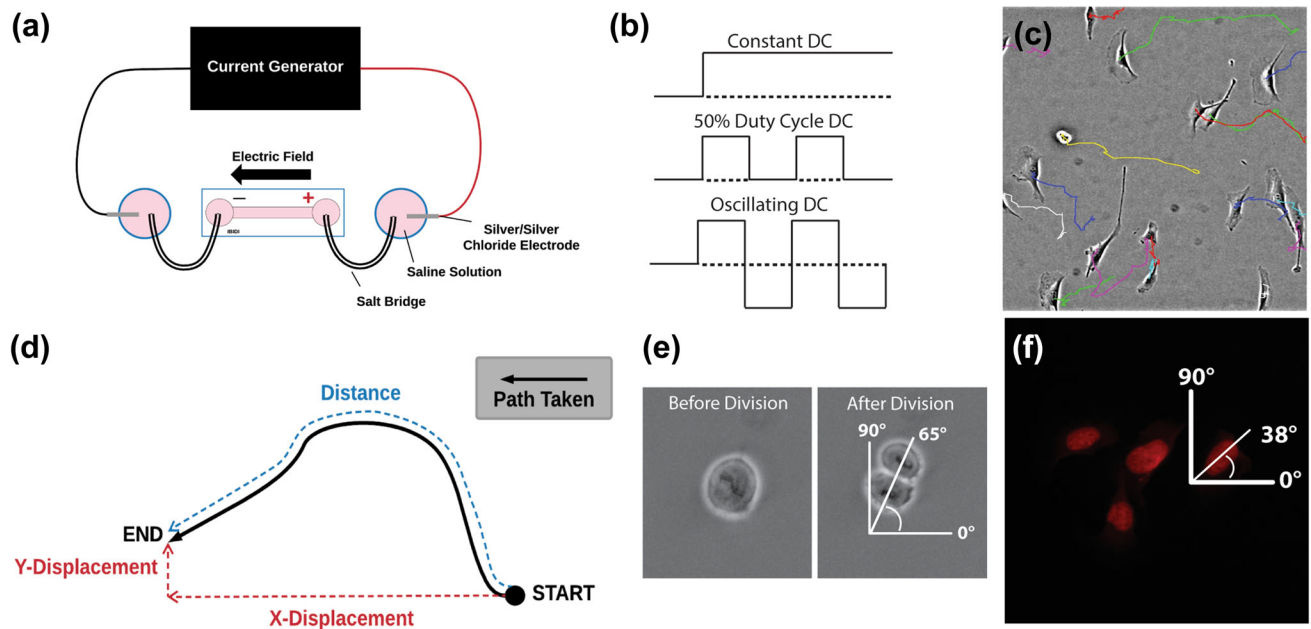


FIGURE 1. (a) Schematic of experimental setup used to apply an exogenous EF through the media to the SCs. (b) Schematic showing three EF waveforms. (c) Phase contrast image of SCs for tracking migration. Previous cell locations are marked with colored lines. (d) Diagram showing definitions of distance, X-displacement and Y-displacement. (e) Fluorescent image of SC nuclei, showing angles measured from horizontal. (f) Diagram showing measurement of the angle of the axis of mitosis.

placement and Y-displacement for each cell. X-displacement and Y-displacement were calculated by subtracting the final position coordinates from the initial position coordinates of each cell. Distance was calculated as the sum of the linear distances between each timepoint (Fig. 1d).

Proliferation rate and angle of the axis of mitosis (referred to as the angle of mitosis) were quantified from the time-lapse image sequences. Proliferation rate was defined as the number of cell divisions in the field of view divided by the number of cells at time 0. The angle of mitosis data was collected from the first image where two daughter cells were apparent (Fig. 1e). In FIJI, a line defined as the axis of mitosis was drawn between the center of both daughter cells, and the angle between this axis and the horizontal was measured (0–90°).

Cell Alignment

Fluorescent Imaging

Cell alignment and morphology data were collected from fluorescent images of fixed SCs after EF exposure. After removing the paraformaldehyde, cells were washed – all washing procedures consisted of rinsing the cells three times with 1× PBS. Next, cells were permeabilized using 0.1% Triton X-100 (Sigma-Aldrich) for 5 min. Cells were again washed and 100 µg/mL RNAase solution was added for 20 min to digest

RNA. Following another wash, propidium iodide (Invitrogen; 1:30) or DAPI (Biotium; 300 nM) in addition to Alexa Fluor 488 Phalloidin (Life Technologies; 1:50) were added to the channel and mixed using a micropipette. After 5 min, the channel slide was washed, and images were captured using the same microscope setup.

Immunofluorescence of Integrin $\beta 1$ was performed in SCs exposed to 500 mV/mm Con EFs and controls. Cells were fixed, permeabilized and washed as described above; however, 0.1% Tween 20 (Sigma-Aldrich) was used for the wash. The anti-integrin $\beta 1$ primary antibody (EMD Millipore; 1:100) was mixed in the channel and left overnight. The primary antibody was aspirated and washed. Blocking buffer (5% FBS in 0.1% Tween 20) was added for 1 h, then the cells were gently rinsed. Alexa Fluor 488 labelled secondary antibody (Jackson ImmunoResearch; 1:1000) was added for 1 h and washed again.

Quantifying SC Alignment and Morphology

Fluorescent images of cell nuclei (Fig. 1f) were uploaded to FIJI and a macro was written to extract the alignment data. The macro applied a bandpass filter to the image, then used the AutoThreshold command using the “minimum dark” setting. The stained pixels were converted to a mask and an ellipse was fit to each stained area with an area greater than 200 pixels. FIJI then exported the angle of the ellipses’ major axis.

Ellipses touching the border of the image were automatically discarded. Finally, FIJI-rendered images displaying ellipses were compared with original fluorescent images to correct errors such as overlapping nuclei. Angles of the long axis were measured (0–180°) with respect to horizontal. Angles larger than 90° were mirrored across the Y-axis such that all measurements of cell alignment were between 0 and 90°.

SC morphology was analyzed using the elongation calculation, which is defined as the ratio of max feret/min feret. Fluorescent images of SC's actin cytoskeleton were analyzed in NIS Elements AR (Version 5.02.00) through a macro utilizing the automated measurement tool. The macro set lower bound threshold values such that only objects with intensity levels above 10–19 and pixel size above 50 were considered. The processing setting, “fill holes”, was set to “on”. All circularity levels (0–1) were considered. The macro did not use measurement frames or ROI; under this condition, the measurement options were changed to exclude objects touching the edge of the image. Once the macro processed the image, the elongation for each identified object was automatically measured. Measurement results for objects that contained more than one cell were manually excluded. Therefore, only the elongation results for objects that were singular, isolated cells were considered.

Statistical Analysis

SC alignment and migration data was collected from three trials ($n = 3$) for all EF waveforms and EF strengths. Migration and alignment data were collected for approximately 100–200 cells for each experimental trial. Fluorescent images (10) of cell nuclei were taken at random locations on the channel slide and used for cell alignment measurements. Overlapping or incomplete nuclei were excluded from the data set. Five random positions were imaged throughout the EF exposure, and the resulting time-lapse image sequences were analyzed to collect migration data.

Statistical significance was determined by comparing the different EF strengths using either ANOVA (for Con EF distance) or nonparametric Kruskal Wallis tests (50% d.c. EF and Osc EF distance, and all EF waveform alignment, X-displacement and Y-displacement) followed by a Bonferroni multiple comparison post-hoc adjustment which compared all EF strengths to controls. Passage number did not have a significant effect on the alignment or migration of the SCs and was removed from the model. A significance level of $\alpha = 0.05$ was used for all statistical analyses.

RESULTS

SC Migration

Exposure to DC EFs was shown to influence mammalian SCs *in vitro*. Changes in SC migration, alignment and morphology were analyzed following 6-h DC EF exposure and were dependent upon EF strength and EF waveform. Each experiment was set up with the voltage gradient oriented horizontally (along the X-axis) with the cathode to the left. Hence X-displacement, or net migration along the X-axis, was either toward the cathode or anode. The Y-direction was perpendicular to the EF. Controls (cells not exposed to EFs) were expected to have a mean X-displacement and Y-displacement of 0 μm .

Migration in Con EF

The mean X-displacement of SCs exposed to Con EFs of 500 mV/mm was $45.0 \pm 60.4 \mu\text{m}$ toward the cathode, while control SCs had a mean X-displacement of $3.0 \pm 42.7 \mu\text{m}$ toward the cathode (Fig. 2a). SC X-displacement in 500 mV/mm EFs was statistically different than control SCs ($p < 0.001$). SC X-displacement in 10 and 75 mV/mm Con EFs was small but was also statistically different from the X-displacement of control SCs ($p < 0.01$, $p < 0.001$ respectively). Statistical analysis revealed that Y-displacement (perpendicular to the EF) was not explained by EF strength, and was very close to the expected mean Y-displacement of 0 μm for all EF strengths tested (Fig. 2b). Con EF exposure was shown to influence SC motility (distance). As field strength increased, distance also tended to increase. The distance traveled by cells exposed to Con EF of 10 ($p < 0.001$), 200 ($p < 0.001$) and 500 mV/mm ($p < 0.001$) were statistically different from control trials (Fig. 2c). Figure 2d shows overlaid traces of cell position during EF exposure, starting from the origin at time = 0 h. A majority (78.7%) of the SCs tracked in 500 mV/mm Con EFs had a cathodal X-displacement. Observation of time-lapse videos revealed many SC projections oriented parallel to the EF were often resorbed shortly after beginning EF stimulation.

Migration in 50% d.c. EF

In 50% d.c. EFs, SCs moved slightly toward the anode at all field strengths with mean X-displacements of: $6.3 \pm 44.7 \mu\text{m}$ at 10 mV/mm, $6.2 \pm 43.6 \mu\text{m}$ at 75 mV/mm, $23.4 \pm 52.2 \mu\text{m}$ at 200 mV/mm and $7.7 \pm 48.6 \mu\text{m}$ at 500 mV/mm. X-displacement was significantly different than control SCs for each EF

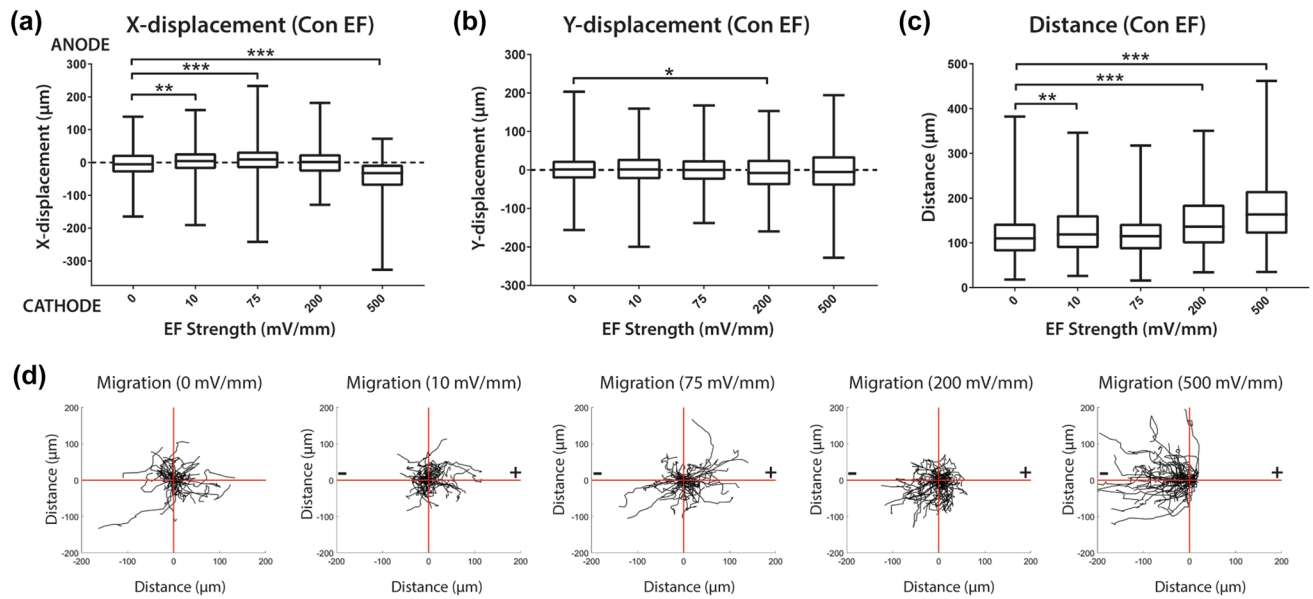


FIGURE 2. SC migration during constant 6-h EF exposure. (a) The mean X-displacement of SCs exposed to 500 mV/mm Con EF was $45.0 \pm 60.4 \mu\text{m}$ toward the cathode compared to $3.0 \pm 42.7 \mu\text{m}$ toward the cathode for controls. At the highest field strength 78.7% of SCs moved toward the cathode, while 56.6% of control SCs moved toward the cathode. (b) Little Y-displacement was observed at any of the field strengths tested. (c) Mean distance traveled by SCs during EF exposure. The distance travelled tended to increase as field strength increased. Significant increase in distance was observed at 10, 200, and 500 mV/mm compared to the control ($p < 0.01$, $p < 0.001$, $p < 0.001$ respectively). (d) Polar plots showing the migration of 50 cells at each EF strength tested. Error bars represent standard deviation.

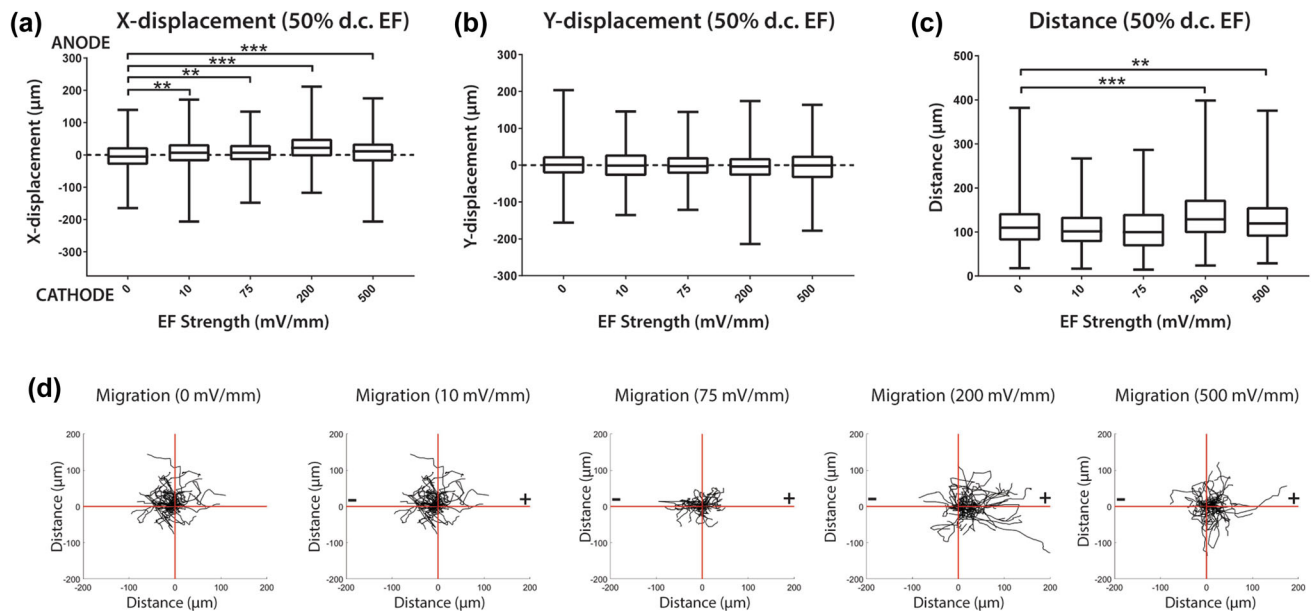


FIGURE 3. SC migration during 50% d.c. EF exposure (15 min on/off). (a) X-displacement was significantly different than controls for SCs in EFs of strengths 10–500 mV/mm ($p < 0.01$, $p < 0.01$, $p < 0.001$, $p < 0.001$ respectively), though the magnitudes of migration were smaller than those observed in 500 mV/mm Con EF. (b) Little Y-displacement was observed at the field strengths tested. (c) Mean distance traveled by SCs during EF exposure. Distance travelled by SCs in 200 and 500 mV/mm 50% d.c. EF was elevated ($140.4 \pm 65.0 \mu\text{m}$, $127.2 \pm 51.7 \mu\text{m}$ respectively) as compared to controls ($115.9 \pm 51.0 \mu\text{m}$). (d) Polar plots of the migration of 50 cells at each EF strength tested. Error bars represent standard deviation.

strength (10 mV/mm, $p < 0.01$; 75 mV/mm, $p < 0.01$; 200 mV/mm, $p < 0.001$; 500 mV/mm, $p < 0.001$) (Fig. 3a). Y-displacement was not explained by field

strength in the statistical model, and the mean Y-displacement was very close to the expected value of $0 \mu\text{m}$ for all field strengths tested (Fig. 3b). An increase in

SC distance was observed at the higher field strengths of 200 and 500 mV/mm ($p < 0.001$; $p < 0.01$) (Fig. 3c).

Migration in Osc EF

SCs exposed to Osc EFs showed little directional response. Directed migration in the X direction was not expected in the Osc EF waveform as there was no permanent cathode or anode. Cells exposed to Osc EFs of 75 mV/mm showed a slight X-displacement of $11.1 \pm 39.9 \mu\text{m}$ to the left that was significantly different than control SCs ($p < 0.01$) (Fig. 4a). Little bias in Y-displacement was seen in the Osc EF waveform (Fig. 4b). There was a statistically significant increase in distance traveled for cells exposed to Osc EFs of 10 ($p < 0.001$), 200 ($p < 0.001$) and 500 mV/mm ($p < 0.001$) compared to control SCs (Fig. 4c).

SC Alignment and Morphology

SC angle was measured from 0 to 90° with respect to the EF or X-axis. Cells were considered to have near-perpendicular alignment if they were oriented within 10° of perpendicular (80–90°). Cells not exposed to EFs were expected to be oriented randomly and therefore have a mean cell angle of 45°. Plotted alignment data was binned every 10°, thus 11.1% of randomly oriented cells would be expected to have near-perpendicular alignment ($10/90 = 0.111$). The rate of cell proliferation and angle of cell division data

were additionally measured from time-lapse images. The mean proliferation rate was $37.9 \pm 12.1\%$ for the controls, and no change in proliferation rate was observed with EF exposure ($p > 0.05$ for all EF strengths) (Supplemental Materials Fig S3). Not surprisingly, the axis of mitosis was biased toward perpendicular with increasing EF strength and appeared consistent with cell alignment data.

Alignment and Morphology in Con EF

Upon application of Con EFs, SCs displayed a bias toward perpendicular alignment (Figs. 5a–5e). In the range of EF strengths tested, increase of perpendicular SC alignment correlated with increased Con EF strength (Fig. 5i). The greatest perpendicular alignment was observed at 500 mV/mm which had a mean angle of $69.9 \pm 19.0^\circ$ compared to $45.3 \pm 26.1^\circ$ of control SCs. After Con EF exposure, SCs exhibited statistically significant changes in alignment at 75 mV/mm ($p < 0.05$) and larger (200 mV/mm, $p < 0.001$; 500 mV/mm, $p < 0.001$) compared to controls. Over 39% of SCs exposed to 500 mV/mm Con EF had near-perpendicular alignment, while 10.7% of control SCs exhibited near-perpendicular alignment. Near-perpendicular alignment of the other field strengths was 25.2% of SCs at 200 mV/mm, 15.0% at 75 mV/mm and 10.8% at 10 mV/mm. Cells exposed to 500 mV/mm Con EFs had more elongated morphologies than control SCs ($p < 0.001$) (Fig. 5j). Mean elongation for

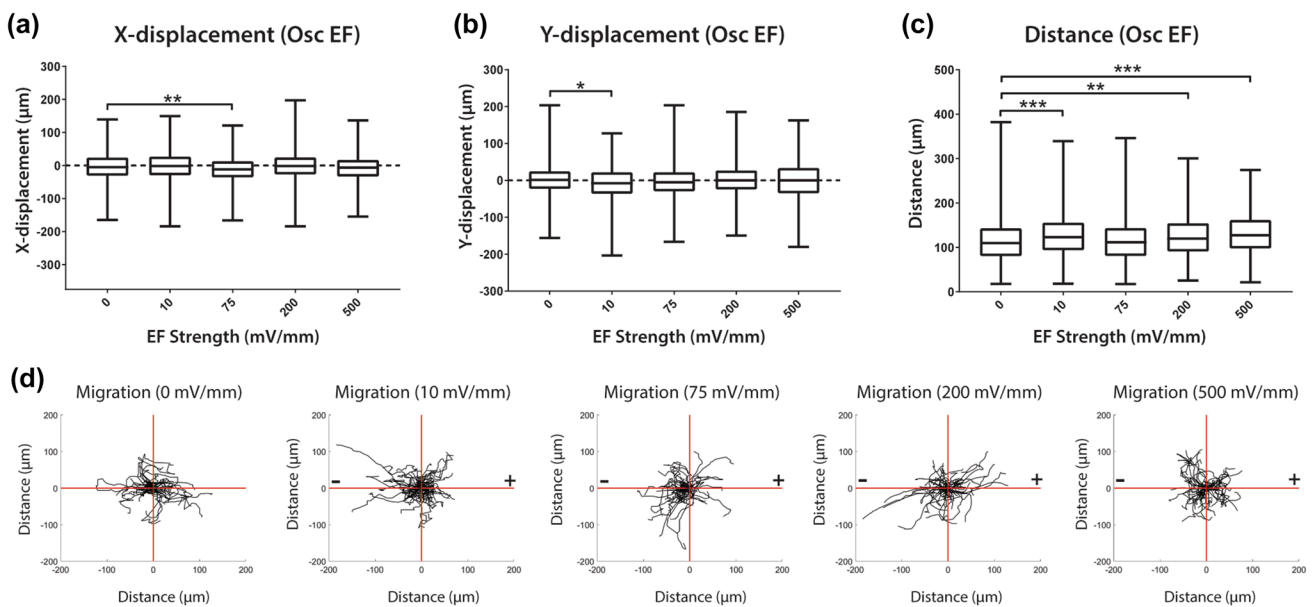


FIGURE 4. SC migration during oscillating EF exposure (field polarity reversed every 15 min). (a) Little X-displacement was observed at the field strengths tested. (b) Little Y-displacement was observed at the field strengths tested. (c) Mean distance travelled by SCs during EF exposure. The distance travelled by SCs increased slightly with increasing Osc EF strength. SCs exposed to Osc EFs of 10, 200, and 500 mV/mm had mean distances ($127.7 \pm 47.2 \mu\text{m}$, $125.0 \pm 48.8 \mu\text{m}$, $130.2 \pm 46.3 \mu\text{m}$ respectively) greater than control SCs ($115.9 \pm 51.0 \mu\text{m}$). (d) Polar plots of the migration of 50 cells at each EF strength tested. Error bars represent standard deviation.

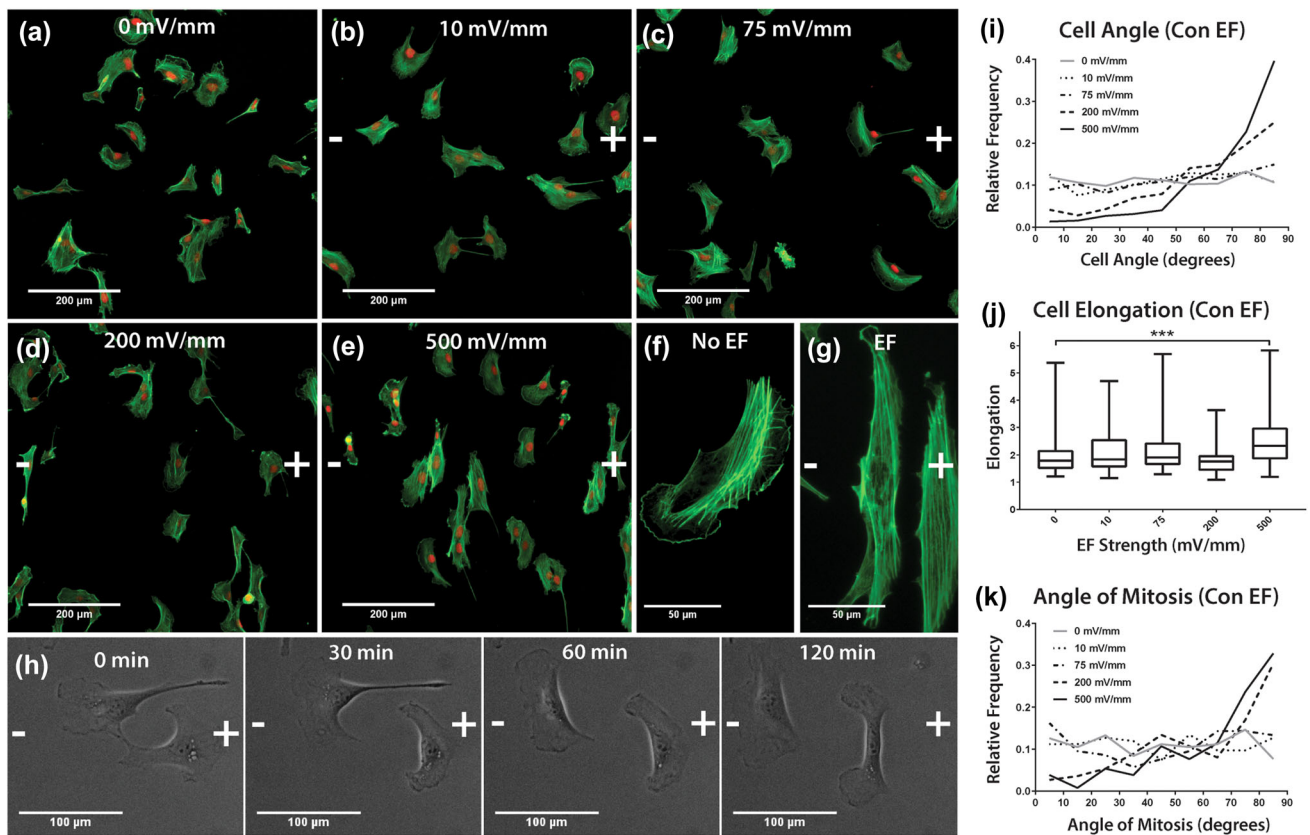


FIGURE 5. SC alignment after 6-h Con EF exposure. EFs ranging from 0 to 500 mV/mm were tested. (a–e) Representative images of SCs after EF exposure. Scale bar 200 μm . Magnified images of (f) control SCs and (g) SCs after exposure to 500 mV/mm Con EF; note the aligned actin fibers in (g) and a less organized fiber orientation in (f). Scale bar 50 μm . (h) Many SCs showed perpendicular alignment within the first 2 h of 500 mV/mm Con EF exposure. Scale bar 100 μm . (i) Histogram of cell alignment at the different EF strengths. Bins for frequency distribution were 10° wide. The angle of cell alignment increased toward perpendicular (90°) as EF strength increased. In constant EF, SCs exhibited significant perpendicular bias at EF strengths of 75, 200, and 500 mV/mm ($p < 0.05$, $p < 0.001$, $p < 0.001$ respectively). (j) SCs exposed to 500 mV/mm Con EF had higher mean cell elongation than control SCs, reflecting the elongated morphology observed after EF exposure ($p < 0.001$). (k) Significant perpendicular orientation of the axis of mitosis was observed in 200 and 500 mV/mm Con EFs ($p < 0.001$ in both). Actin shown in green, nucleus in red.

SCs exposed to 500 mV/mm Con EFs was 2.56 ± 0.97 , while mean elongation of control SCs was 1.93 ± 0.63 . The angle of mitosis also exhibited significant perpendicular orientation in 200 ($60.5 \pm 23.8^\circ$) and 500 mV/mm EFs ($64.9 \pm 22.1^\circ$) ($p < 0.001$ in both) (Fig. 5k).

No changes in intracellular symmetry or localization of I β 1 were observed in EF stimulated SCs vs. controls (Fig. 6). Regardless of 500 mV/mm Con EF exposure time (15 min–6 h), I β 1 staining was diffuse and had no apparent cathodal or anodal bias.

Alignment and Morphology in 50% d.c. EF

SC alignment in 50% d.c. EFs followed a similar trend to the alignment of SC in Con EFs with perpendicular cell alignment correlating with higher field strength (Figs. 7a–7f). The greatest alignment was observed at the highest EF strength, with a mean cell

angle of $63.4 \pm 22.4^\circ$. There was statistically significant alignment at field strengths of 75 ($p < 0.001$), 200 ($p < 0.001$), and 500 mV/mm ($p < 0.001$) compared to control SCs. 27.6% of SCs exposed to a 500 mV/mm 50% d.c. EF had near-perpendicular alignment. The percentage of cells with near-perpendicular alignment at the remaining field strengths was: 20.5% at 200 mV/mm, 12.2% at 75 mV/mm and 13.0% at 10 mV/mm. No significant changes in morphology were observed in SCs exposed to 50% d.c. EFs compared with control SCs ($p > 0.05$) (Fig. 7g). Perpendicular orientation of the angle of mitosis was observed in 200 ($52.5 \pm 27.4^\circ$) and 500 mV/mm EFs ($59.5 \pm 24.9^\circ$) ($p < 0.05$; $p < 0.001$) (Fig. 7h).

Alignment and Morphology in Osc EF

During Osc EF exposure, SCs again aligned perpendicular at high field strengths (Figs. 8a–8f). Sig-

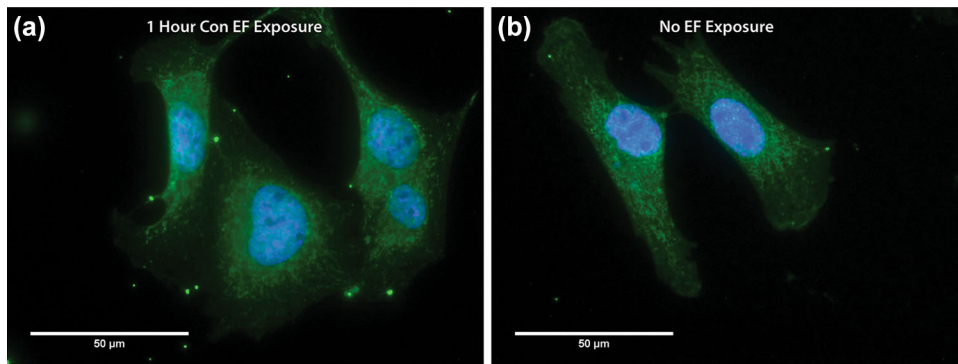


FIGURE 6. Representative images of Integrin $\beta 1$ distribution in SCs after (a) 1-h exposure in 500 mV/mm Con EF and (b) no EF exposure. Asymmetry in the $I\beta 1$ distribution was not detected after EF exposures of 15 min, 30 min, 1 h, 3 h or 6 h. $I\beta 1$ shown in green, DAPI shown in blue. Scale bar 50 μm .

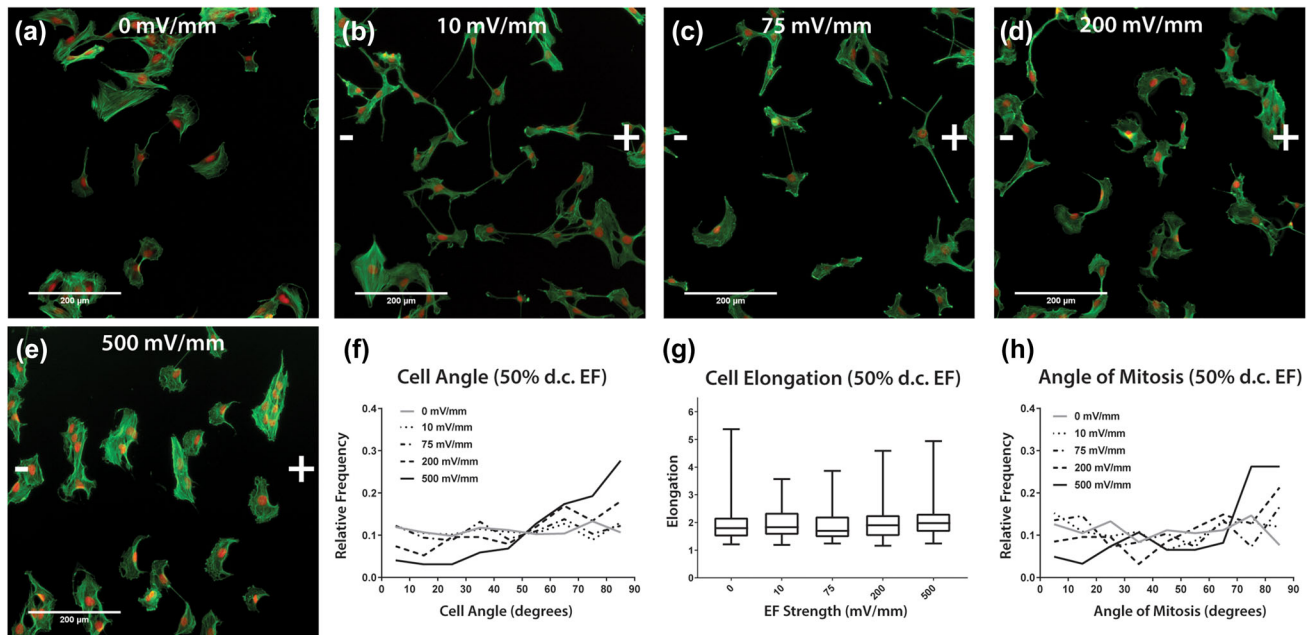


FIGURE 7. SC alignment after 6-h 50% d.c. EF exposure. EFs ranging from 0 to 500 mV/mm were tested. (a–e) Representative images after 50% d.c. EF exposure show perpendicular alignment. (f) Histogram of cell alignment by EF strength. Bins used in the frequency distribution were 10° wide. The angle of cell alignment increased toward perpendicular (90°) as EF strength increased. In 50% d.c. EF SCs exhibited significant perpendicular bias at EF strengths of 75, 200, and 500 mV/mm ($p < 0.001$, $p < 0.001$, and $p < 0.001$ respectively). (g) SCs exposed to 50% d.c. EFs showed little change in cell morphology compared with control SCs ($p = 0.28$). (h) Significant perpendicular orientation of the axis of mitosis was observed in 200 and 500 mV/mm 50% d.c. EFs ($p < 0.05$, $p < 0.001$). Error bars represent standard deviation. Scale bar 200 μm . Actin shown in green, nucleus in red.

nificant perpendicular alignment was only observed at 500 mV/mm ($p < 0.001$). SCs in this group had a mean cell angle of $54.3 \pm 25.4^\circ$. 18.3% of SCs exposed to 500 mV/mm 50% d.c. EFs were near-perpendicular. The percentage of cells that had near-perpendicular alignment in the remaining field strengths were close to the expected value of 11.1% (12.3% of SCs at 200 mV/mm, 12.9% at 75 mV/mm and 10.8% at 10 mV/mm). There was a significant change in cell morphology in SCs exposed to 500 mV/mm Osc EFs; the mean elongation observed in SCs exposed to 500 mV/mm Osc

EFs was 2.28 ± 0.71 compared to 1.93 ± 0.63 for control SCs ($p < 0.001$) (Fig. 8g). The angle of mitosis had a slight perpendicular orientation in 500 mV/mm EFs (Fig. 8h). The mean angle of mitosis was $53.7 \pm 24.7^\circ$ ($p < 0.001$).

DISCUSSION

In this work, we studied the role of DC EFs and their variant waveforms on RT4 SC migration, orientation and morphology. The impetus for screening

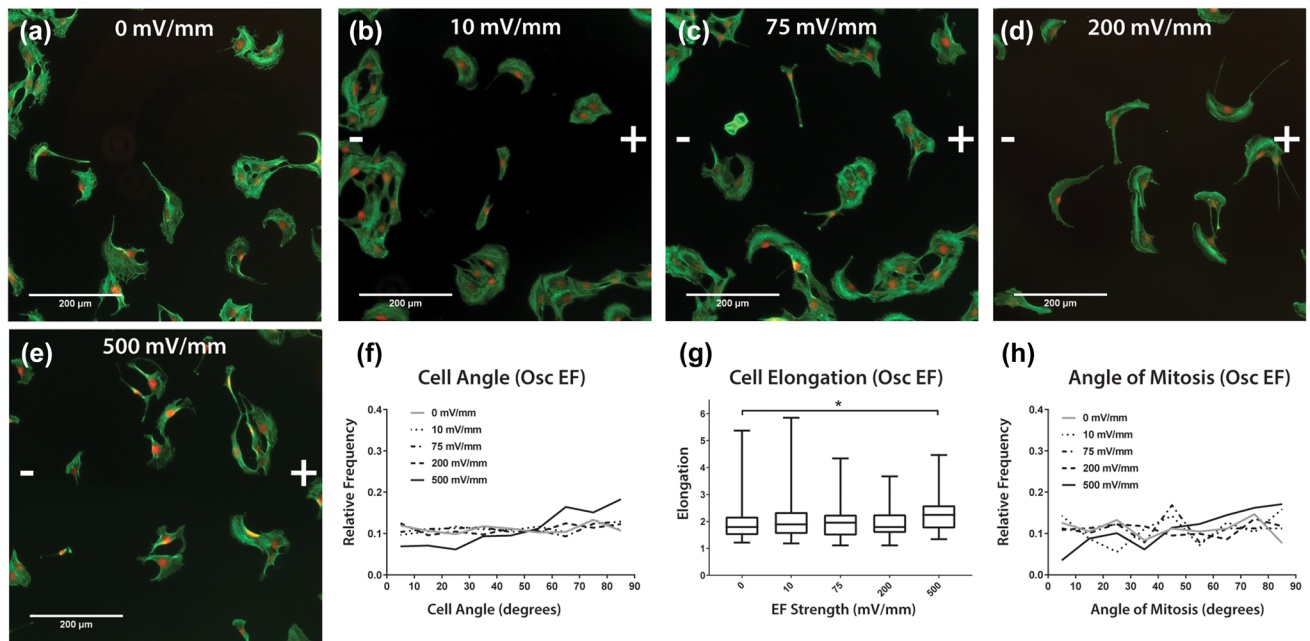


FIGURE 8. SC alignment after 6-h Osc EF exposure. EFs ranging from 0 to 500 mV/mm were tested. (a–e) Representative images of SCs after Osc EF exposure; note the slight bias toward perpendicular cell alignment in (e). (f) Histogram of cell alignment by EF strength. Bins used in the frequency distribution were 10° wide. The angle of cell alignment increased toward perpendicular (90°) as EF strength increased. In Osc EFs, SCs exhibited significant perpendicular bias at 500 mV/mm ($p < 0.001$). (g) SCs exposed to Osc EFs displayed changes in morphology at field strengths of 500 mV/mm ($p < 0.05$). (h) Significant perpendicular orientation of the axis of mitosis was observed in 500 mV/mm Osc EFs ($p < 0.001$). Error bars represent standard deviation. Scale bar 200 μm. Actin shown in green, nucleus in red.

these stimulation regimes was to obtain exploratory data to justify these waveforms for implantable devices targeted for PNS regeneration. Previous experiments have only examined SCs in constant DC fields. However, constant DC may induce cytotoxicity *in vivo* due to the accumulation of electrochemical byproducts near the electrodes. A 50% duty cycle DC was a logical choice for both reduced power consumption and for eliciting unidirectional responses. A similar duty cycle was tested in cats with spinal injuries.⁴⁰ We also employed a unique oscillating DC stimulation protocol that was modeled from the oscillating field stimulator (OFS), a technology developed by Borgens *et al.* for promoting axon regeneration after spinal cord injury.^{8,35} The oscillating field stimulation is constant DC, except the polarity reverses every 15 min. It was found that if polarity reversal occurred at less than 60-min intervals, cathodal attraction would not be negated by anodal repulsion during polarity switching.²⁴ The effective outcome of this oscillatory field is bidirectional growth. This polarity change further negates the pH changes at the electrodes.⁵ The EF magnitudes selected in our experiments (10–500 mV/mm) are physiologically relevant and consistent with previous cellular EF studies.^{1,30,36}

Changes in cellular orientation during EF stimulation were striking and rapid (Video 1). SCs displayed

highly perpendicular alignment to the field vector, and the degree of alignment was proportional to the EF strength. At high strength EFs of 500 mV/mm, SC reorientation was observed within the first hour of EF exposure with continuous current (constant and oscillating waveforms). SC processes oriented parallel to the EF upon start of the stimulation often retracted, a phenomenon also described in neurons.²⁹ This response timeframe corroborates findings in mouse 3T3 fibroblasts, which reoriented perpendicular to an applied 550 mV/mm EF within 2 h.⁶ Not surprisingly, the constant waveform resulted in the most pronounced cellular reorientation, but bias toward perpendicular alignment was also noted in the 50% duty cycle and oscillating waveforms. Almost 40% of cells exposed to 500 mV/mm Con EF had complete perpendicular alignment (80–90°). Near perpendicular alignment decreased to 24.2% in 50% d.c. EF and 18.3% in Osc EF. The degree of alignment was less in the 50% duty cycle scenario but perpendicular alignment was still observed at EFs as low as 75 mV/mm. The oscillating waveform resulted in the weakest cellular reorientation with the highest EF strength of 500 mV/mm inducing realignment. Interestingly, the rate of cell proliferation was not statistically significant between groups (Fig S3) but the axis of mitosis was orthogonal to the field vector at higher EF strengths

(Figs. 5k, 7h, 8h). Zhao *et al.* reported oriented mitosis in corneal epithelial cells and suggested EFs affect the alignment of the mitotic spindles, which determine the orientation of the cleavage plane.⁴³ The morphology of EF stimulated SCs were also more elongated, and exhibited a bipolar configuration. This effect was dependent on EF strength. Overall, the morphological characteristics were similar to mouse fibroblasts, often displaying large cathode-facing lamellipodia which facilitated migration.¹⁶

EF exposure induced distinct cathodal migration only in 500 mV/mm Con EFs. In 500 mV/mm constant DC stimulation, cathodal galvanotaxis was measured to be $7.5 \pm 10.1 \mu\text{m/h}$. Weaker EF magnitudes as well as 50% duty cycle and oscillating stimulation resulted in minimal cell displacement. Cells exposed to 50% d.c. EFs tended to move slightly toward the anode. EF exposure also tended to enhance cell motility, and SCs exposed to 500 mV/mm Con EFs showed a 47% increase in migration compared to controls.

EF-induced migration, growth and reorientation are well-known phenomena which occur in many cell types originating from the ectoderm.^{6,9,13,24} Cellular reorientation perpendicular to the applied EFs has been observed in hippocampal neurons,³² astrocytes⁶ and neural derived crest cells.^{13,26,39} Primary chick sympathetic and dorsal root ganglia neurons also extend neurites orthogonal to the EFs when using the same uncoated polyethylene channel slides and field intensities.^{29,30} However, this is the first demonstration of rapid perpendicular alignment in SCs. In earlier studies, Koppes *et al.* did not find any SC morphology or alignment changes at fields less than 100 mV/mm.²⁰ Only at 12 h post-stimulation was some parallel alignment observed (25–75 mV/mm range).¹⁹ In another report, Yao *et al.* found directed migration towards the anode in rat SCs.⁴¹ We speculate differences in substratum charge and cell seeding may explain the conflicting data. For instance, Koppes *et al.* used a much higher cell density (32,000 vs. 4,000 cells/cm²). A higher cell density can affect alignment *via* contact inhibition or biochemical gradients generated by neighboring cells. A delayed observation time could have permitted cellular reorientation. Here, we observed an almost immediate perpendicular realignment after EF exposure, especially in fields above 200 mV/mm. The anodal migration reported by Yao *et al.* was observed on positively charged poly-L-lysine (PLL) substrates. It has been previously shown that substrate charge can influence or even reverse cellular orientation in the presence of an EF.³³ We mitigated substratum related effects by using uncoated polyethylene-based slides (net negative charge per conversations with manufacturer). However, we also assessed

substratum related effects by culturing SCs on the polyethylene slides coated with positively charged PLL. Using 500 mV/mm constant DC stimulation, we found that X-displacement of SCs towards the cathode was much smaller on PLL ($4.3 \pm 39.4 \mu\text{m}$) vs. uncoated polyethylene slides ($45.0 \pm 60.4 \mu\text{m}$) (Supplemental Materials Fig S2A). The net distance traveled was also noticeably less on the positively charged PLL (Fig S2C) but perpendicular alignment was maintained on both substrate types (Fig S2D). Competing charge effects between the substrate and charged membrane proteins may dampen/enhance the EF-induced electrophoretic effect, ultimately affecting cell motility. Thus, when interpreting and comparing data, the substrate charge/type is an important variable to consider.

The underlying mechanisms of signal transduction are not well understood. One purported explanation for cellular reorientation is the asymmetric redistribution of charged surface receptors induced by the applied DC fields.²⁵ Evidence of this electro-osmotic effect moving charged moieties within the cell has been shown in concanavalin A receptors³¹ as well as acetylcholine receptors.²⁷ In non-neuronal cells, Brown and Lowe showed more diffuse yet asymmetric distribution of the integrin $\alpha 5$ subunit in murine fibroblasts exposed to EFs.⁹ Other theories describing molecular mechanisms of EF signal transduction include the polarization of ion transport proteins or changes to the transmembrane potential.²⁸ However, we did not detect any changes in the spatial expression of I β 1 in SCs subjected to the highest levels of constant DC stimulation (Fig. 6). Because of the strong alignment response seen in SCs, future work may analyze the distribution of membrane receptor proteins that have displayed responses to EFs in other cell types.

A limitation of the study was the use of the RT4 SC line rather than primary cells. The appropriateness of the RT4 as a model was validated against primary SCs obtained from rats (Supplemental Materials Fig S1). We found primary SCs were comparably responsive to EFs, with cell motility being increased compared to RT4 line. Perpendicular alignment was also observed in primary SCs with the mean cell angle ($64.9 \pm 20.3^\circ$) being marginally less than RT4 SCs ($69.9 \pm 19.0^\circ$) ($p < 0.05$). We suspect the muted motility of the RT4 line may be attributed to phenotypic changes that occur from prolonged 2-D *in vitro* culture even though the RT4 cells expressed typical SC markers (data not shown). Primary SCs also de-differentiate after injury and take on a more reparative role.² Such phenotypic adaptations may explain a more migratory state. However, the overall differences, while detectable, were relatively small between the cell line and primary cultures. These results suggest that RT4 cells may be a

suitable surrogate for characterizing EF-mediated effects while providing a more homogeneous population of cells.

Our experimental results show EF-induced migratory, alignment, and morphological changes in SCs are dependent on field intensity and waveform properties. SC responses were most dramatic in constant DC fields, but notable alignment was also observed with 50% duty cycle and oscillating EFs. This is the first report of discontinuous or alternating DC fields having an effect on SC motility and orientation. While the biological significance of these findings is unclear, there is strong evidence to support further *in vivo* experiments with EFs. For instance, in neuron-SC co-cultures, neurons seeded with EF stimulated SCs show enhanced neurite outgrowth and faster neurite extension.²⁰ Neurites also follow the local cellular topography when grown atop SC monolayers.³⁴ EF stimulated SCs produce more growth factors¹⁹ and upregulate specific genes associated with focal adhesion and actin cytoskeleton signaling pathways, both of which influence cell motility.⁴¹ Adult SCs also divide along an axis that is parallel to the nerve.²³ Thus, it is foreseeable that strategic application of EFs after PNI may enhance SC migration into the lesion and encourage the formation of an aligned cellular “template” (i.e., similar to bands of Bungner) to facilitate axon pathfinding and regeneration. Implantable devices may be developed to deliver these EFs, and we have outlined findings from stimulation regimes that have proven to be safe *in vivo*. However, additional stimulation profiles (such as alternating current) may also be explored. The presented methods provide a framework for manipulating waveform parameters to further modulate SC behavior.

ELECTRONIC SUPPLEMENTARY MATERIAL

The online version of this article (<https://doi.org/10.1007/s10439-019-02259-4>) contains supplementary material, which is available to authorized users.

ACKNOWLEDGMENTS

This study was completed at the Center for Paralysis Research with funding provided by the State of Indiana. The authors thank Megan Saenger and Bhavani Gopalakrishnan for their assistance with cell culture.

REFERENCES

- ¹Alexander, J. K., B. Fuss, and R. J. Colello. Electric field-induced astrocyte alignment directs neurite outgrowth. *Neuron Glia Biol.* 2:93–103, 2006.
- ²Arthur-Farraj, P. J., M. Latouche, D. K. Wilton, S. Quintes, E. Chabrol, A. Banerjee, A. Woodhoo, B. Jenkins, M. Rahman, M. Turmaine, G. K. Wicher, R. Mitter, L. Greensmith, A. Behrens, G. Raivich, R. Mirsky, and K. R. Jessen. c-Jun reprograms Schwann cells of injured nerves to generate a repair cell essential for regeneration. *Neuron* 75:633–647, 2012.
- ³Bonazzi, D., and N. Minc. Dissecting the molecular mechanisms of electrotactic effects. *Adv. Wound Care* 3:139–148, 2014.
- ⁴Borgens, R. B. Electrically mediated regeneration and guidance of adult mammalian spinal axons into polymeric channels. *Neuroscience* 91:251–264, 1999.
- ⁵Borgens, R. B., K. R. Robinson, J. W. Venable, and M. E. McGinnis. Artificially controlling axonal regeneration and development by applied electric fields. In: *Electric Fields in Vertebrate Repair*. New York: Alan R. Liss, 1989, pp. 164–165.
- ⁶Borgens, R. B., R. Shi, T. J. Mohr, and C. B. Jaeger. Mammalian cortical astrocytes align themselves in a physiological voltage gradient. *Exp. Neurol.* 128:41–49, 1994.
- ⁷Borgens, R., J. Toombs, A. Blight, M. McGinnis, M. Bauer, W. Widmer, and J. Cook. Effects of applied electric-fields on clinical cases of complete paraplegia in dogs. *Restor. Neurol. Neurosci.* 5:305–322, 1993.
- ⁸Borgens, R. B., J. P. Toombs, G. Breur, W. R. Widmer, D. Waters, A. M. Harbath, P. March, and L. G. Adams. An imposed oscillating electrical field improves the recovery of function in neurologically complete paraplegic dogs. *J. Neurotrauma* 16:639–657, 1999.
- ⁹Brown, M. J., and L. M. Loew. Electric field directed fibroblast locomotion involves cell surface molecular reorganization and is calcium independent. *J. Cell Biol.* 127:117–128, 1994.
- ¹⁰Bunge, R. P. The role of the Schwann cell in trophic support and regeneration. *J. Neurol.* 242:S19–S21, 1994.
- ¹¹Bunge, R. P., and M. B. Bunge. Interrelationship between Schwann cell function and extracellular matrix production. *Trends Neurosci.* 6:499–505, 1983.
- ¹²Chang, H. F., Y. S. Lee, T. K. Tan, and J. Y. Cheng. Pulsed DC electric field-induced differentiation of cortical neural precursor cells. *PLoS ONE* 11:e0158133, 2016.
- ¹³Cooper, M. S., and R. E. Keller. Perpendicular orientation and directional migration of amphibian neural crest cells in dc electrical fields. *Proc. Natl Acad. Sci. U.S.A.* 81:160–164, 1984.
- ¹⁴Hall, S. M. Regeneration in cellular and acellular autografts in the peripheral nervous system. *Neuropathol. Appl. Neurobiol.* 12:27–46, 1986.
- ¹⁵Hall, S. M. The effect of inhibiting Schwann cell mitosis on the re-innervation of acellular autografts in the peripheral nervous system of the mouse. *Neuropathol. Appl. Neurobiol.* 12:401–414, 1986.

- ¹⁶Huang, Y. J., J. Samorajski, R. Kreimer, and P. C. Searson. The influence of electric field and confinement on cell motility. *PLoS ONE* 8:e59447, 2013.
- ¹⁷Jaffe, L. F. The role of ionic currents in establishing developmental pattern. *Philos. Trans. R. Soc. Lond. B Biol. Sci.* 295:553–566, 1981.
- ¹⁸Jessen, K. R., and R. Mirsky. The repair Schwann cell and its function in regenerating nerves. *J. Physiol.* 594:3521–3531, 2016.
- ¹⁹Koppes, A. N., A. L. Nordberg, G. Paolillo, N. Goodsell, H. Darwish, L. Zhang, and D. M. Thompson. Electrical stimulation of Schwann cells promotes sustained increases in neurite outgrowth. *Tissue Eng. Part A* 20:494–506, 2013.
- ²⁰Koppes, A. N., A. M. Seggio, and D. M. Thompson. Neurite outgrowth is significantly increased by the simultaneous presentation of Schwann cells and moderate exogenous electric fields. *J. Neural Eng.* 8:1–13, 2011.
- ²¹Li, R., Z. Liu, Y. Pan, L. Chen, Z. Zhang, and L. Lu. Peripheral nerve injuries treatment: a systematic review. *Cell Biochem. Biophys.* 68:449–454, 2014.
- ²²Mackinnon, S. E., and A. L. Dellon. Nerve repair and nerve grafts. In: *Surgery of the Peripheral Nerve*, edited by S. E. Mackinnon. New York: Thieme, 1988.
- ²³Martin, J. R., and H. D. Webster. Mitotic Schwann cells in developing nerve: their changes in shape, fine structure, and axon relationships. *Dev. Biol.* 32:417–431, 1973.
- ²⁴McCaig, C. D. Spinal neurite reabsorption and regrowth *in vitro* depend on the polarity of an applied electric field. *Development* 100:31–41, 1987.
- ²⁵McLaughlin, S., and M. M. Poo. The role of electro-osmosis in the electric-field-induced movement of charged macromolecules on the surfaces of cells. *Biophys. J.* 34:85–93, 1981.
- ²⁶Nuccitelli, R., and C. A. Erickson. Embryonic cell motility can be guided by physiological electric fields. *Exp. Cell Res.* 147:195–201, 1983.
- ²⁷Orida, N., and M. Poo. Electrophoretic movement and localisation of acetylcholine receptors in the embryonic muscle cell membrane. *Nature* 275:31–35, 1978.
- ²⁸Ozkucur, N., S. Perike, P. Sharma, and R. Funk. Persistent directional cell migration requires ion transport proteins as direction sensors and membrane potential differences in order to maintain directedness. *BMC Cell Biol.* 12:1–13, 2011.
- ²⁹Pan, L., and R. B. Borgens. Perpendicular organization of sympathetic neurons within a required physiological voltage. *Exp. Neurol.* 222:161–164, 2010.
- ³⁰Pan, L., and R. B. Borgens. Strict perpendicular orientation of neural crest-derived neurons *in vitro* is dependent on an extracellular gradient of voltage. *J. Neurosci. Res.* 90:1335–1346, 2012.
- ³¹Poo, M., J. W. Lam, N. Orida, and A. W. Chao. Electrophoresis and diffusion in the plane of the cell membrane. *Biophys. J.* 26:1–22, 1979.
- ³²Rajnicek, A. M., N. A. R. Gow, and C. D. McCaig. Electric field-induced orientation of rat hippocampal neurons *in vitro*. *Exp. Physiol.* 77:229–232, 1992.
- ³³Rajnicek, A. M., K. R. Robinson, and C. D. McCaig. The direction of neurite growth in a weak DC electric field depends on the substratum: contributions of adhesivity and net surface charge. *Dev. Biol.* 203:412–423, 1998.
- ³⁴Seggio, A. M., A. Narayanaswamy, B. Roysam, and D. M. Thompson. Self-aligned Schwann cell monolayers demonstrate an inherent ability to direct neurite outgrowth. *J. Neural Eng.* 7(4):046001, 2010.
- ³⁵Shapiro, S., R. Borgens, R. Pascuzzi, K. Roos, M. Groff, S. Purvines, R. B. Rodgers, S. Hagy, and P. Nelson. Oscillating field stimulation for complete spinal cord injury in humans: a phase 1 trial. *J. Neurosurg. Spine* 2:3–10, 2005.
- ³⁶Shi, R., and R. B. Borgens. Three-dimensional gradients of voltage during development of the nervous system as invisible coordinates for the establishment of embryonic pattern. *Dev. Dyn.* 202:101–114, 1995.
- ³⁷Siemionow, M., and G. Brzezicki. Current techniques and concepts in peripheral nerve repair. *Int. Rev. Neurobiol.* 87:141–172, 2009.
- ³⁸Son, Y. J., and W. J. Thompson. Schwann cell processes guide regeneration of peripheral axons. *Neuron* 14:125–132, 1995.
- ³⁹Stump, R. F., and K. R. Robinson. Xenopus neural crest cell migration in an applied electrical field. *J. Cell Biol.* 97:1226–1233, 1983.
- ⁴⁰Talat, K., S. Sayers, and N. Chauhan. Effect of applied electric field on astrocytic scar formation after spinal cord injury. In: *Electricity and Magnetism in Biology and Medicine*, edited by F. Bersani. Boston: Springer, 1999, pp. 887–890.
- ⁴¹Yao, L., Y. Li, J. Knapp, and P. Smith. Exploration of molecular pathways mediating electric field-directed Schwann cell migration by RNA-seq. *J. Cell. Physiol.* 230:1515–1524, 2015.
- ⁴²Yao, L., and L. Yongchao. The role of direct current electric field-guided stem cell migration in neural regeneration. *Stem Cell Rev.* 12:365–375, 2016.
- ⁴³Zhao, M., J. V. Forrester, and C. D. McCaig. A small physiological electric field orients cell division. *Proc. Natl. Acad. Sci. U.S.A.* 96:4942–4946, 1999.

Publisher's Note Springer Nature remains neutral with regard to jurisdictional claims in published maps and institutional affiliations.